

CONF-9109104--1

TEXTURES AND MORPHOLOGIES OF CHEMICAL VAPOR
DEPOSITED (CVD) DIAMOND

CONF-9109104--1

DE92 001969

R.E. Clausing, L. Heatherly, L. L. Horton,
E. D. Specht, G. M. Begun, and Z. L. Wang*

Oak Ridge National Laboratory
P.O. Box 2008
Oak Ridge, Tennessee 37831-6093 USA

Phone: 615-574-5084
FAX: 615-574-7659

DISCLAIMER

This report was prepared as an account of work sponsored by an agency of the United States Government. Neither the United States Government nor any agency thereof, nor any of their employees, makes any warranty, express or implied, or assumes any legal liability or responsibility for the accuracy, completeness, or usefulness of any information, apparatus, product, or process disclosed, or represents that its use would not infringe privately owned rights. Reference herein to any specific commercial product, process, or service by trade name, trademark, manufacturer, or otherwise does not necessarily constitute or imply its endorsement, recommendation, or favoring by the United States Government or any agency thereof. The views and opinions of authors expressed herein do not necessarily state or reflect those of the United States Government or any agency thereof.

*University of Tennessee, Knoxville.

"The submitted manuscript has been authored by a contractor of the U.S. Government under contract No. DE-AC05-84OR21400. Accordingly, the U.S. Government retains a nonexclusive, royalty-free license to publish or reproduce the published form of this contribution, or allow others to do so, for U.S. Government purposes."

MASTER

DISTRIBUTION OF THIS DOCUMENT IS UNLIMITED

TEXTURES AND MORPHOLOGIES OF CHEMICAL VAPOR DEPOSITED (CVD) DIAMOND

R. E. Clausing, L. Heatherly, L. L. Horton,
E. D. Specht, G. M. Begun, and Z. L. Wang
Oak Ridge National Laboratory
P.O. Box 2008, Oak Ridge, TN 37831-6093, USA

SUMMARY

The textures, surface morphologies, structural perfection, and properties of diamond films grown by activated chemical vapor deposition (CVD) vary greatly with the growth conditions. The evolution of two commonly observed polycrystalline morphologies, which give rise to $\langle 110 \rangle$ textures, will be described as well as the development of four films grown to produce $\langle 100 \rangle$, $\langle 111 \rangle$, and "near $\langle 100 \rangle$ " textures with various combinations of growth facets. These films were grown to test models of texture development.

Films free of twins, microtwins, and stacking faults are deposited when only $\{100\}$ facets are permitted to grow. In polycrystalline materials, special conditions must be met to avoid the formation of planar defects at the peripheries of individual crystallites. The planar defects grow from $\{111\}$ or mixed microfaceted surfaces. Twinning plays an important role in growth of $\{111\}$ faceted surfaces. The films have been characterized with Raman spectroscopy, x-ray diffraction, transmission electron microscopy (TEM), scanning electron microscopy (SEM), and optical methods.

INTRODUCTION

The structure and thereby the properties of diamonds obtained by activated chemical vapor deposition (CVD) processes depend strongly on the nucleation and

growth conditions. By specifying and adjusting these conditions, there is an opportunity to optimize the properties of diamond for specific applications. Not only is crystal perfection/defect structure important, but grain boundary properties, crystallite shape, orientation and surface finish are critical since most applications will use polycrystalline films. It is essential to understand, in detail, how the growth processes determine the structure of CVD diamond materials. This paper will explore the relationship between growth, surface, and bulk structure.

The primary purpose of this paper is to test the van der Drift competitive growth model¹ for texture development. In this model, randomly oriented nuclei grow competitively on the substrate. Those crystallites for which the most rapidly growing direction is perpendicular to the plane of the substrate grow taller and gradually envelope the less favorably oriented crystallites. Van der Drift called this "the model of the survival of the fastest growing crystallites."

Crystallite shapes can be used to determine growth rates in various crystallographic directions. Figure 1 shows cubo-octahedral shapes for crystallites based on growth along the $\langle 100 \rangle$ and $\langle 111 \rangle$ crystal directions. We define the ratio of the growth rate in the $\langle 100 \rangle$ to the growth rate in the $\langle 111 \rangle$ as R. The R values associated with each of the cubo-octahedral shapes is given under each drawing. R values range from 0.58 for a cube to 1.73 for an octahedron. The longest direction in a cube is the $\langle 111 \rangle$ diagonal, the longest direction in the octahedron is the $\langle 100 \rangle$ diagonal, and the longest direction in the cubo-octahedron ($R = 0.87$) is the $\langle 110 \rangle$ direction. We have been able to grow individual crystallites with the full

range of shapes shown in Fig. 1. Figure 2 shows cubes grown with $R = 0.6$ and octahedra grown with $R = \sim 1.7$. The van der Drift theory would predict that, for films grown with $R = 0.6$, a $\langle 111 \rangle$ texture would develop; for $R = 0.87$, a $\langle 110 \rangle$ texture would develop; and for $R = 1.7$, a $\langle 100 \rangle$ texture would develop. For most films reported in the literature, the R values range from 0.8 to 1.1. It is not surprising that measurements for such films often indicate $\langle 110 \rangle$ textures, because the longest crystal dimension, hence the fastest growing direction is close to $\langle 110 \rangle$.

There is another model which can explain the growth of material with $\langle 110 \rangle$ textures. It was proposed by Meakin² that the formation of twins and microtwins in diamond cubic materials could result in rapid growth in the $\langle 110 \rangle$ direction. Fast growth in the $\langle 110 \rangle$ direction leaves a crystal bounded by the slower growing faces, i.e., the $\{100\}$ and $\{111\}$. A major advantage of this model is that it provides a mechanism for relatively rapid growth on $\{111\}$ faces by virtue of the presence of nucleation sites at every microtwin boundary. There are three parallel sets of $\{111\}$ planes intersecting each $\{111\}$ face; since $\{111\}$ is the diamond twin plane, the intersecting $\{111\}$ planes provide many opportunities for nucleation of microtwins.

A secondary objective of this work is to relate the crystal perfection to the crystal surface from which the bulk material was formed. Prior work³⁻⁷ has shown that polycrystalline material grown with a predominance of $\{111\}$ facets is likely to have a large number of twins, stacking faults, and other planar defects, while material grown from $\{100\}$ facets has dislocations and point defects but not stacking faults or twins. Work by Geis⁸ and Badzian⁹ on single crystals has also shown that growth on

{111} facets is likely to contain many more defects than growth on {100} facets. We have recently shown that, within a single crystallite in a polycrystalline film, zones which formed by growth from {100} facets are free of planar defects while zones grown from {111} facets contain large numbers of planar defects.¹⁰⁻¹² By controlling the growth conditions, and thereby the texture, it is possible to control the surface morphologies so as to influence the nature and extent to which crystal defects are included in the final product.

EXPERIMENTAL TECHNIQUES

The films reported in this paper were grown by the hot-filament activated CVD process described previously.³ The gas compositions and substrate temperatures were varied over a wide range of values to produce the morphologies described in the paper. Films were grown on (100) single crystal silicon substrates. Scanning electron microscopy was performed with a Hitachi model S-800 microscope. A special technique involving the use of fractured films and a combination of scanning and transmission electron microscopy in an analytical transmission electron microscope (TEM) has been used to relate topographical features to bulk structure. This technique has been described recently.⁹ Philips CM30 and Philips CM12 analytical microscopes were used in these studies.

X-ray diffraction and Raman spectroscopy studies were conducted according to procedures described previously.^{3,13}

RESULTS AND DISCUSSION

This section is divided into three parts, each one devoted to a family of textures. Due to space limitations, emphasis is given to the results of SEM, although TEM, Raman spectroscopy, and x-ray diffraction analyses played important roles in developing the underlying understanding of the development of these textures.

<110> Textured Films

The <110> texture is commonly observed in polycrystalline diamond films including microcrystalline films. Figure 3a shows the appearance of a microcrystalline film which has no well-defined crystal faces and yet has a well-defined <110> texture. We have shown previously^{3,5} that the structure contains a high concentration of defects, including microtwins. If the microtwins are an integral part of the growth process, it is reasonable to expect that the texture of this material would be <110>.² Figure 3b shows the appearance of a hot filament CVD film typical of those most often reported in the literature. It has well-defined crystal facets, easily identified as square {100} and triangular {111} faces. For the film of Fig. 3b, the growth rate ratios, R, appear to be about 0.85 as estimated by the shape of the crystallites. This would, according to the van der Drift model, cause the <110> texture to develop as is observed.

Other films provide further evidence of twins and their association with {111} facets as seen in Fig. 4. Figure 4a shows a pair of penetration twins growing on a {100} face. The smooth facets of the twins are {100} faces while the three-fold faceted faces are {111} faces. The {111} faces are rough and have an appearance

consistent with the growth facilitated by microtwinning. Figure 4b is a high magnification SEM image of a {111} face surrounded by {100} faces. Again, the three-fold traces of microtwins on the {111} facet can be seen.

Above we have seen the characteristics of two commonly observed polycrystalline $\langle 110 \rangle$ textures. In both cases the $\langle 110 \rangle$ direction is the fastest growing direction and in both cases twins and microtwins are apparent in the bulk material. In the case of the well-faceted structure of the film seen in Fig. 3b, either the van der Drift or the Meakin model could explain the development of the texture.

We shall introduce terminology to concisely describe the morphology and texture of a film as follows. The facets exposed on the surface will be listed in order of abundance followed by the texture. Thus, the film shown in Fig. 3b would be called {111} {100} $\langle 110 \rangle$. This would indicate that {111} faces are the most abundant, but {100} faces are also present and the texture is $\langle 110 \rangle$.

$\langle 100 \rangle$ Textured Films

Thick films were grown under the conditions for which the octahedral shaped crystals formed, i.e., $R \approx 1.7$. Such a film is shown in Fig. 5a. The texture is $\langle 100 \rangle$ with {111} facets. This material has no {100} faces in the surface morphology. The growth rate in the $\langle 100 \rangle$ direction is so fast that the associated {100} faces become vanishingly small. The {111} faces are very rough and microfaceted with many features that have 3-fold symmetry. Transmission electron microscopy shows that the material contains a high concentration of microtwins and stacking faults, although the individual crystallites clearly retain their identity.¹⁰ If R is decreased to about 1.1, we

obtain the material shown in Fig. 5b. This is highly textured material with the $\langle 100 \rangle$ directions of the crystallites oriented 10 to 15° away from the normal to the substrate. The structure is highly columnar and is free of stacking faults and twins in the centers of the grains at the surface. The evolution of this material has been described previously⁵ in some detail. The initial nucleation has no preferred orientation; however, competitive growth soon leads to this near $\langle 100 \rangle$ texture. The growth ratio, R , is somewhat too low to completely account for the development of the $\langle 100 \rangle$ texture with the simple van der Drift model. However, the general pattern of development is consistent with the van der Drift model. The deviation from the van der Drift model may be due to failure of the van der Drift assumption of an infinite surface diffusion rate.

Another $\langle 100 \rangle$ textured film has been grown in order to examine, in detail, the relationship between surface morphology and bulk structure. Since the columnar shape of the grains suggests that the entire crystal is growing perpendicular to the substrate, an R was selected to yield relatively large $\{100\}$ faces parallel to the substrate while maintaining the $\{111\}$ faces at the periphery of the grains. Figure 6a shows the topography of the growing crystallites. The bulk material can be divided into zones according to whether they were formed on $\{100\}$ or $\{111\}$ facets as shown; the dotted lines define the boundary between the $\{100\}$ and $\{111\}$ regions. Using the technique described in detail elsewhere,¹¹ the film was fractured and examined in an analytical microscope in which SEM images could be obtained to reveal the topography and a suitable grain could be selected for TEM. Figure 6b is

a dark-field image of a grain oriented in the manner shown in Fig. 6a. Detailed analysis of this image shows that the zone grown from the $\{100\}$ facet is free of stacking faults and twins while the zone grown from $\{111\}$ facets contains a high concentration of microtwins. Examination of conventionally prepared TEM specimens in plan view (a section parallel to the substrate, Fig. 6c) of the sample confirms the defect model. The square areas are free from twins while the surrounding regions which grew from $\{111\}$ facets are filled with microtwins. These results clearly indicate a growth process in which microtwins are formed as material is added to $\{111\}$ but not $\{100\}$ planes.

$\{100\}$ $\langle 111 \rangle$ Films

Films were grown with R near 0.6 to produce $\langle 111 \rangle$ textured material with $\{100\}$ facets as would be predicted by the van der Drift model. Figure 7 is a SEM image which reveals the triangular pyramids enclosed by $\{100\}$ facets and topped with small $\{111\}$ facets. This film was not grown to great thicknesses because the growth rate was very slow; therefore, the $\langle 111 \rangle$ texture is not all pervasive. Twins are observed and not all of the tri-pyramids are perfectly oriented. Nevertheless, we believe this film provides good support for the van der Drift model. Although space limitations prevent detailed descriptions, we have also grown films which are not completely explained by the van der Drift model. Films with a $\langle 111 \rangle$ texture and large $\{111\}$ facets parallel to the substrate, $\langle 110 \rangle$ textured material with only $\{100\}$ faces, and an additional form of the $\{100\}$ $\langle 111 \rangle$ textured films which have large growth steps on the $\{100\}$ facets. These films are still under study.

CONCLUSIONS

In summary, we have shown that van der Drift's model can be used to guide the development of diamond films with a wide variety of textures and that the shape of individual crystallites can be used to predict the texture which will develop. We have further shown that the internal structure of the films is a direct result of the growth process on individual facets. For the films thus far studied, growth on {111} facets always leads to the inclusion of twins and microtwins while growth on {100} facets prevents the formation of twins and stacking faults within the grains. Thus, films free of twins, microtwins, and stacking faults can be deposited when only {100} facets are permitted to grow. Several films with only {100} facets have been described. The fully developed {100} $\langle 100 \rangle$ texture has been shown to avoid planar defects even at the boundaries of individual crystallites.

ACKNOWLEDGMENT

This research was sponsored by the U.S. Army Strategic Defense Command under Interagency Agreement No. 1896-1562-A1 with the Department of Energy, the Exploratory Studies Program of Oak Ridge National Laboratory, and the Division of Materials Sciences of the U.S. Department of Energy under contract DE-AC05-84OR21400 with Martin Marietta Energy Systems, Inc.

REFERENCES

1. A. van der Drift, Philips Res. Rep., 22 (1967) 267.
2. D. Meakin, J. Stoemenos, D. Miglierate, and N. A. Economou, J. Appl. Phys., 61 (1987) 5031.

3. R. E. Clausing, L. Heatherly, Jr., K. L. More, and G. M. Begun, *Surf. Coat. Technol.* 39/40 (1989) 199-210.
4. R. E. Clausing, L. Heatherly, Jr., and E. D. Specht, *Diamond and Diamond-Like Films and Coatings*, NATO-ASI Series B: Physics, Plenum Publishing Co., New York, 1991, in press.
5. R. E. Clausing, L. Heatherly, E. D. Specht, and K. L. More, *Proc. 2nd Int. Conf. of New Diamond Science and Technology*, R. Messier (ed.), Materials Research Society, Boston, 1991, pp. 575-80.
6. A. V. Heatherington, C.J.H. Wort, and P. Southworth, *J. Mater. Res.*, 5 (1990) 1591-94.
7. J. L. Kaae, P. K. Gantzel, J. Chin, and W. P. West, *J. Mater. Res.*, 5 (1990) 1480-89.
8. M. W. Geis, *Proc. SDIO/IST-ONR Diamond Technology Initiative Symposium*, Crystal City, Virginia, 1989.
9. A. R. Badzian, T. Badzian, X. H. Wang, and T. M. Hartnett, *2nd Int. Conf. of the New Diamond Science and Technology*, R. Messier (ed.), Materials Research Society, Boston, 1991, pp. 549-56.
10. Z. L. Wang, J. Bentley, R. E. Clausing, L. Heatherly, and L. L. Horton, *Applications of Diamond Films and Related Materials*, Y. Tzeng et al. (eds.), Elsevier Science Publishing B.V., 1991, pp. 489-94.

11. Z. L. Wang, J. Bentley, R. E. Clausing, L. Heatherly, and L. L. Horton, Proc. 49th Ann. Meet. of EMSA, G. W. Bailey et al. (eds.), San Francisco Press, 1991.
12. Z. L. Wang, J. Bentley, R. E. Clausing, L. Heatherly, and L. L. Horton, paper 12.24 this meeting.
13. E. D. Specht, R. E. Clausing, and L. Heatherly, J. Mater. Res., 5 (1990) 2351.

List of Figures

Fig. 1. Cubo-octahedral shapes for different $\langle 100 \rangle / \langle 111 \rangle$ growth rate ratios, R. The R values for each shape are listed under the drawing.

Fig. 2. SEM micrographs of the crystallite shapes produced with growth rate ratios of 0.6 and 1.7.

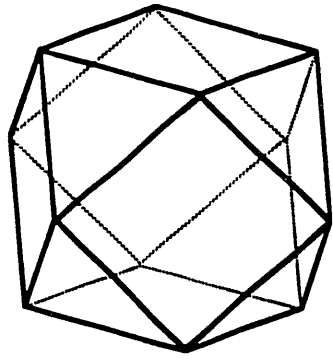
Fig. 3. SEM micrographs of crystal structures with a $\langle 110 \rangle$ texture: (a) microcrystalline film; (b) film with predominantly $\{111\}$ facets plus some $\{100\}$ facets.

Fig. 4. High magnification SEM micrographs showing twinning features: (a) penetration twins, smooth facets are $\{100\}$; rough, three-fold faceted facets are $\{111\}$; (b) extremely high magnification image of a $\{111\}$ face surrounded by $\{100\}$ faces. Note the three-fold traces of the microtwins on $\{111\}$.

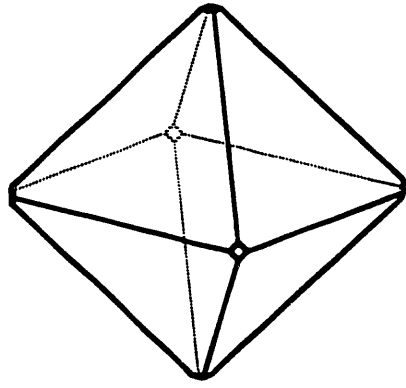
Fig. 5. SEM micrographs of films with a $\langle 100 \rangle$ texture: (a) film grown with $R = 1.7$ yields $\{111\}$ facets; (b) film grown with $R = 1.1$ yields $\{100\}$ facets, the $\langle 100 \rangle$ texture is $\sim 10\text{-}15^\circ$ off of the substrate normal.

Fig. 6. Structure of a $\{100\} \{111\} \langle 100 \rangle$ film: (a) schematic of topography, where dotted lines define the boundary between $\{100\}$ and $\{111\}$ regions; (b) dark-field TEM image of a region oriented as in 6a; (c) plan-view TEM image, note square areas ($\{100\}$) are free of defects while the surrounding areas ($\{111\}$ growth zones) are heavily defected.

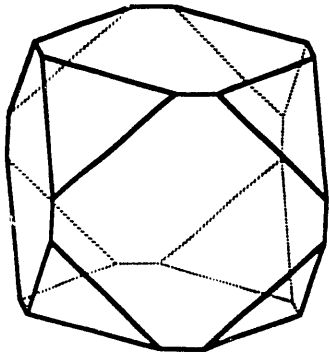
Fig. 7. SEM image of $\{100\}$ films with a $\langle 111 \rangle$ texture. Note the triangular pyramids enclosed by $\{100\}$ facets topped with small $\{111\}$ facets.



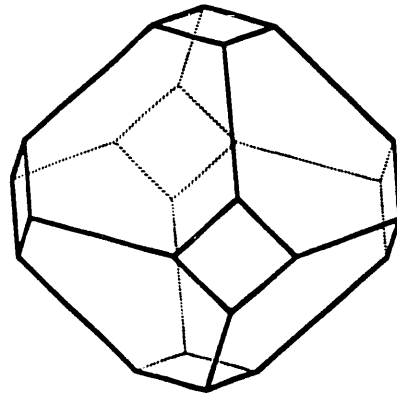
0.87



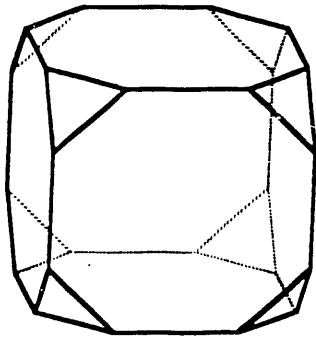
1.65



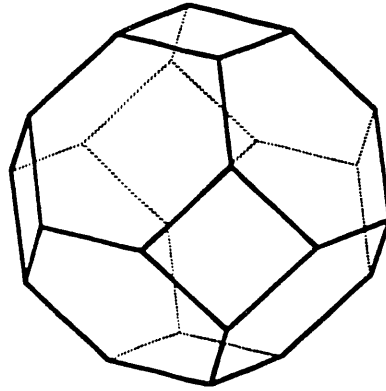
0.8



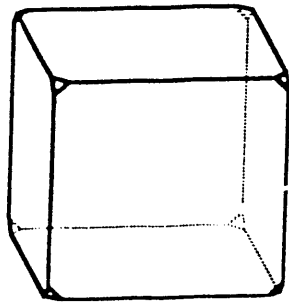
1.3



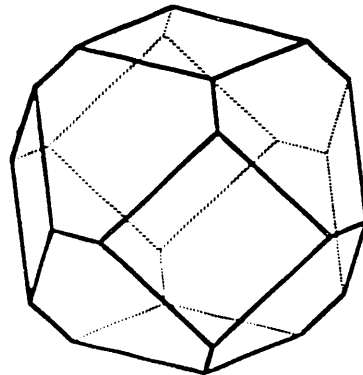
0.7



1.15

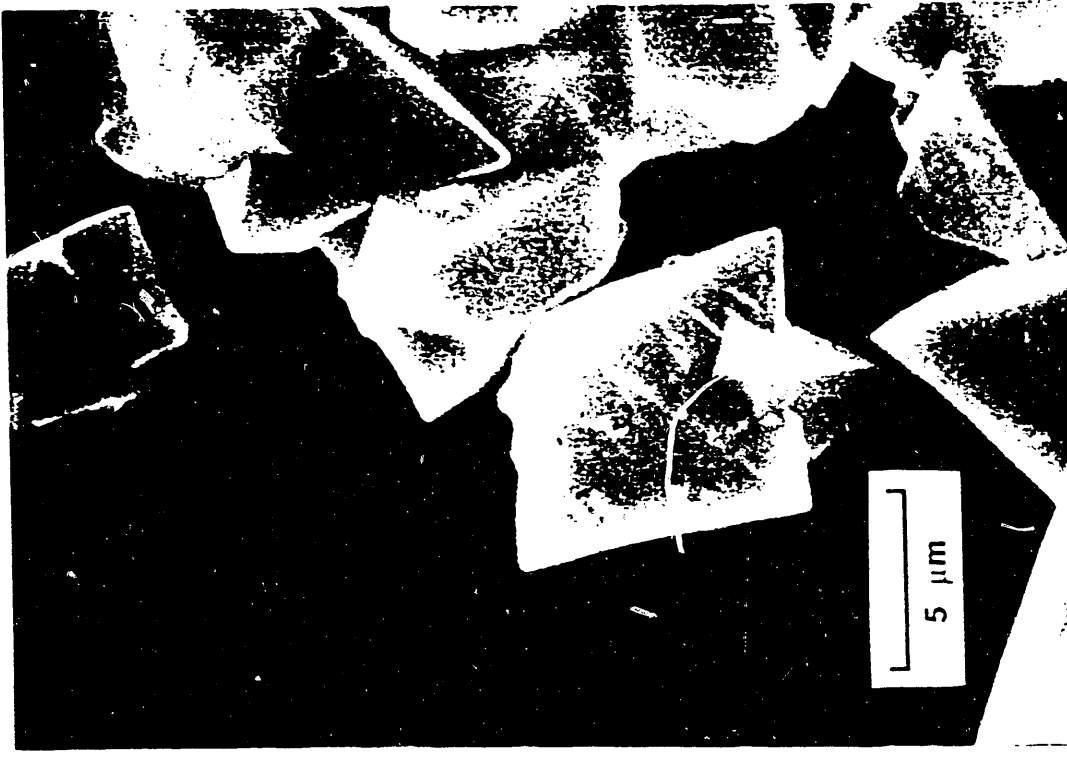


0.6



1.0

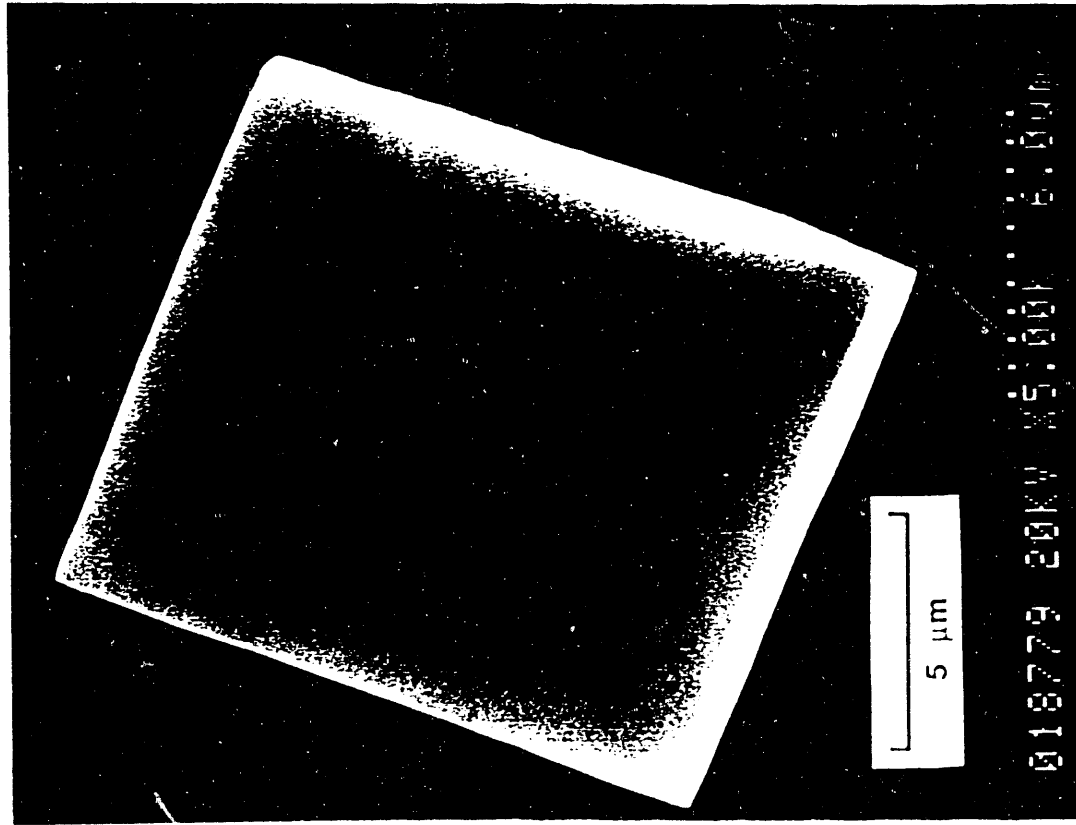
Fig. 1



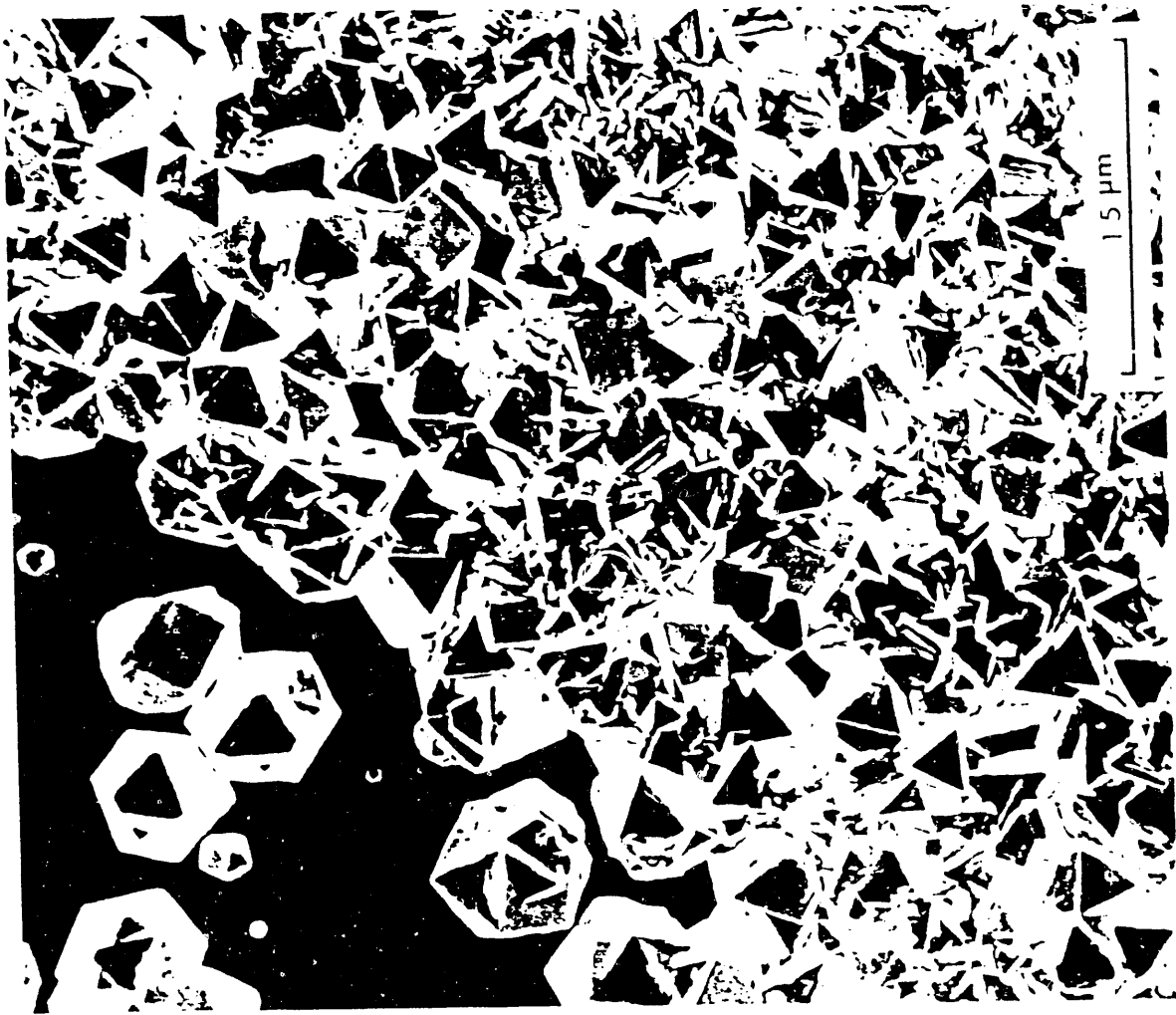
R=1.7

oml

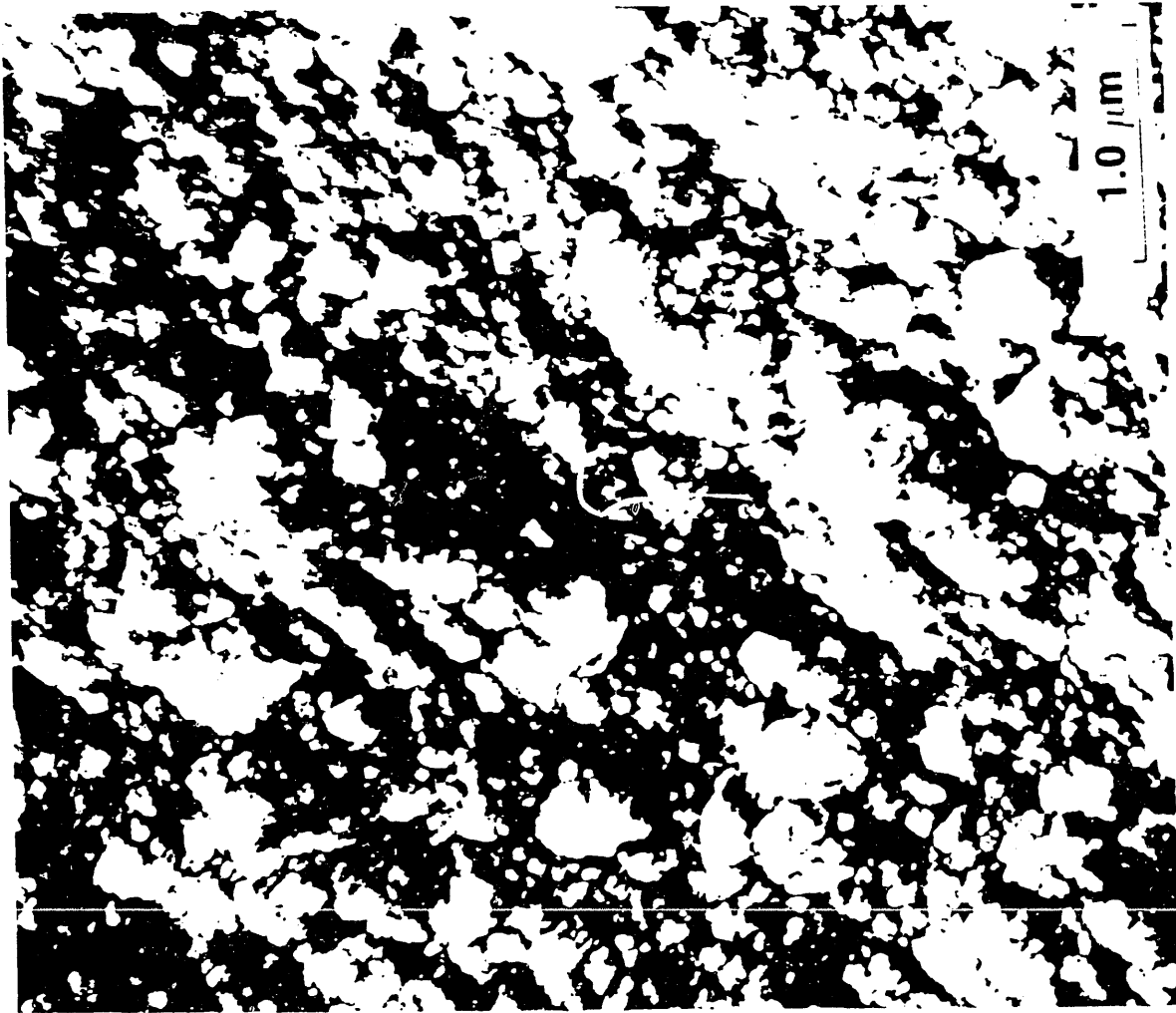
Fin 2



R=0.6



b



a

Fig 3



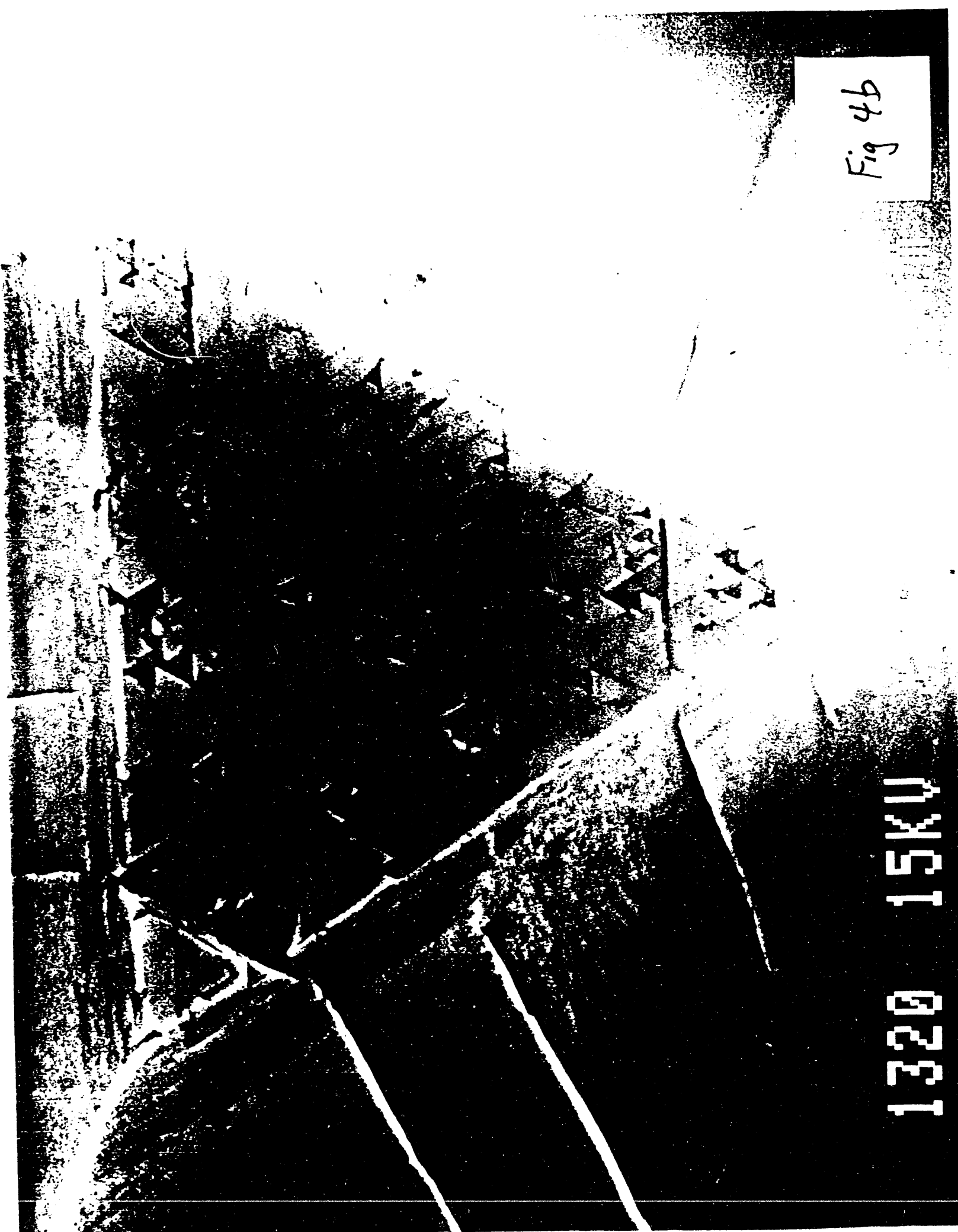
X30.0K.1.00um

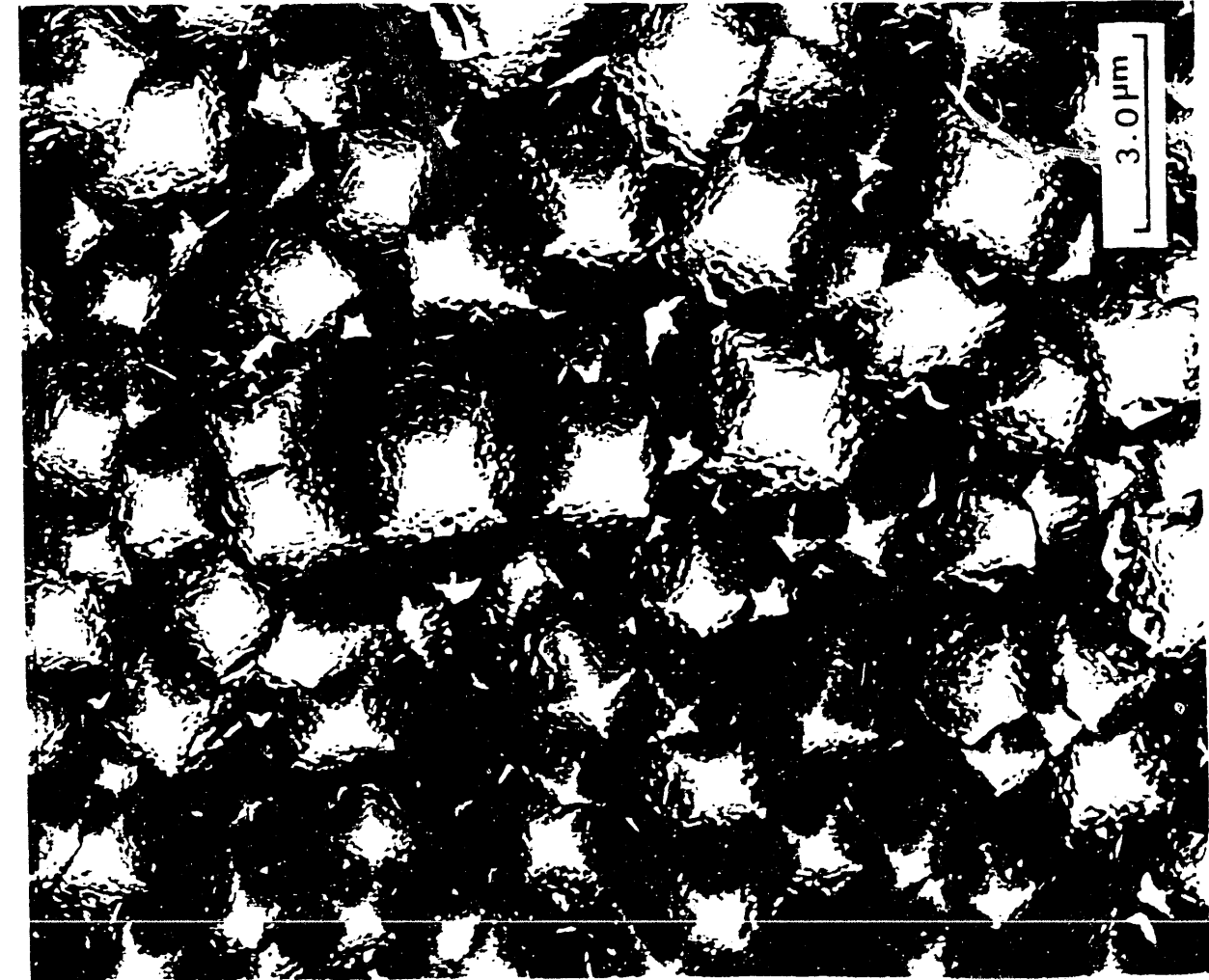
0mm

Fig 4a

Fig 4b

1320 15KV





6



4

Figs

a

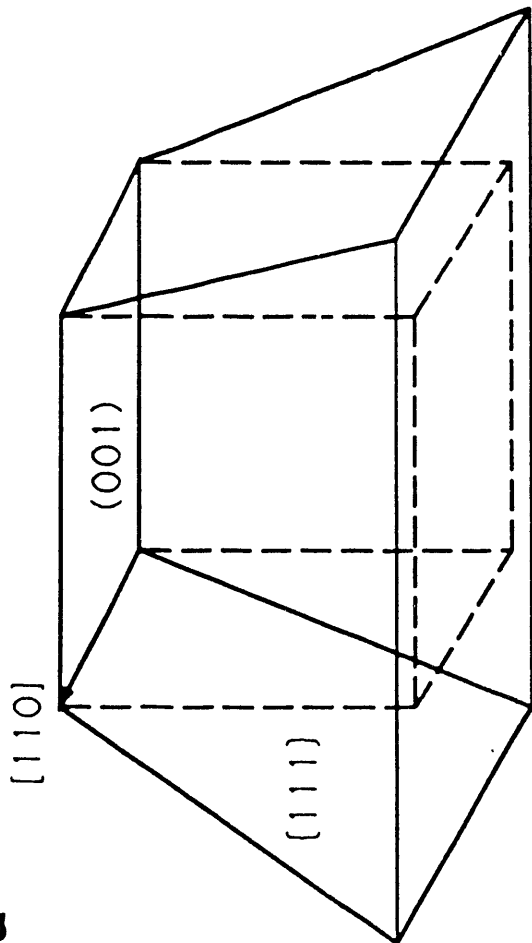
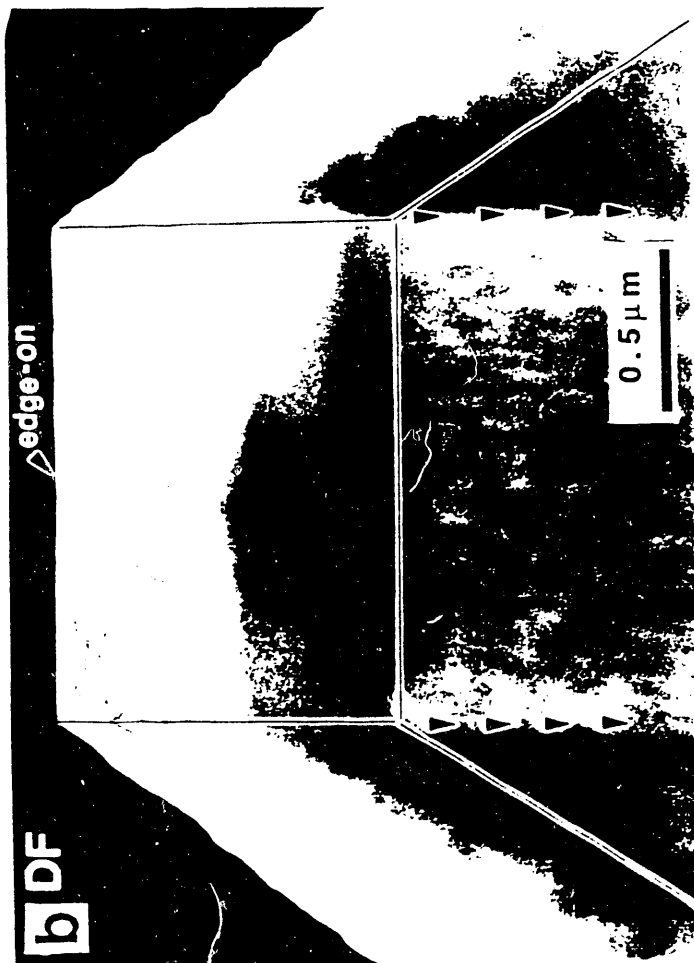
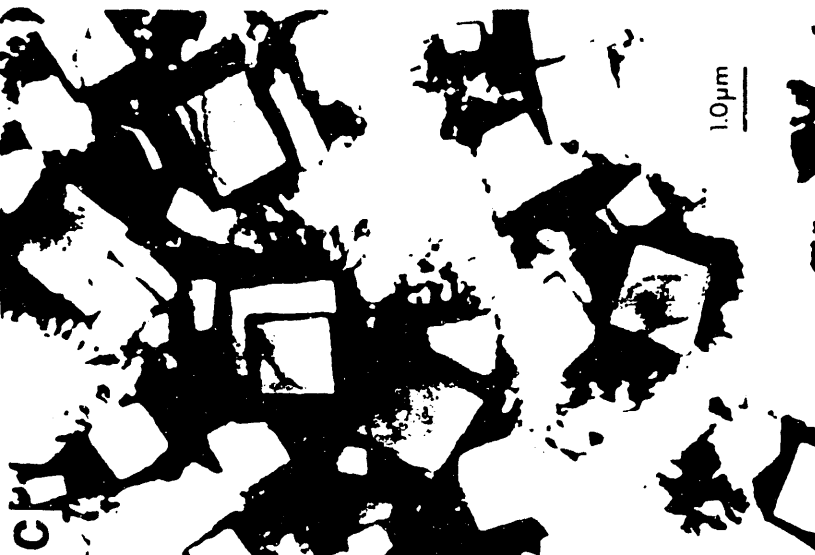


Fig 6



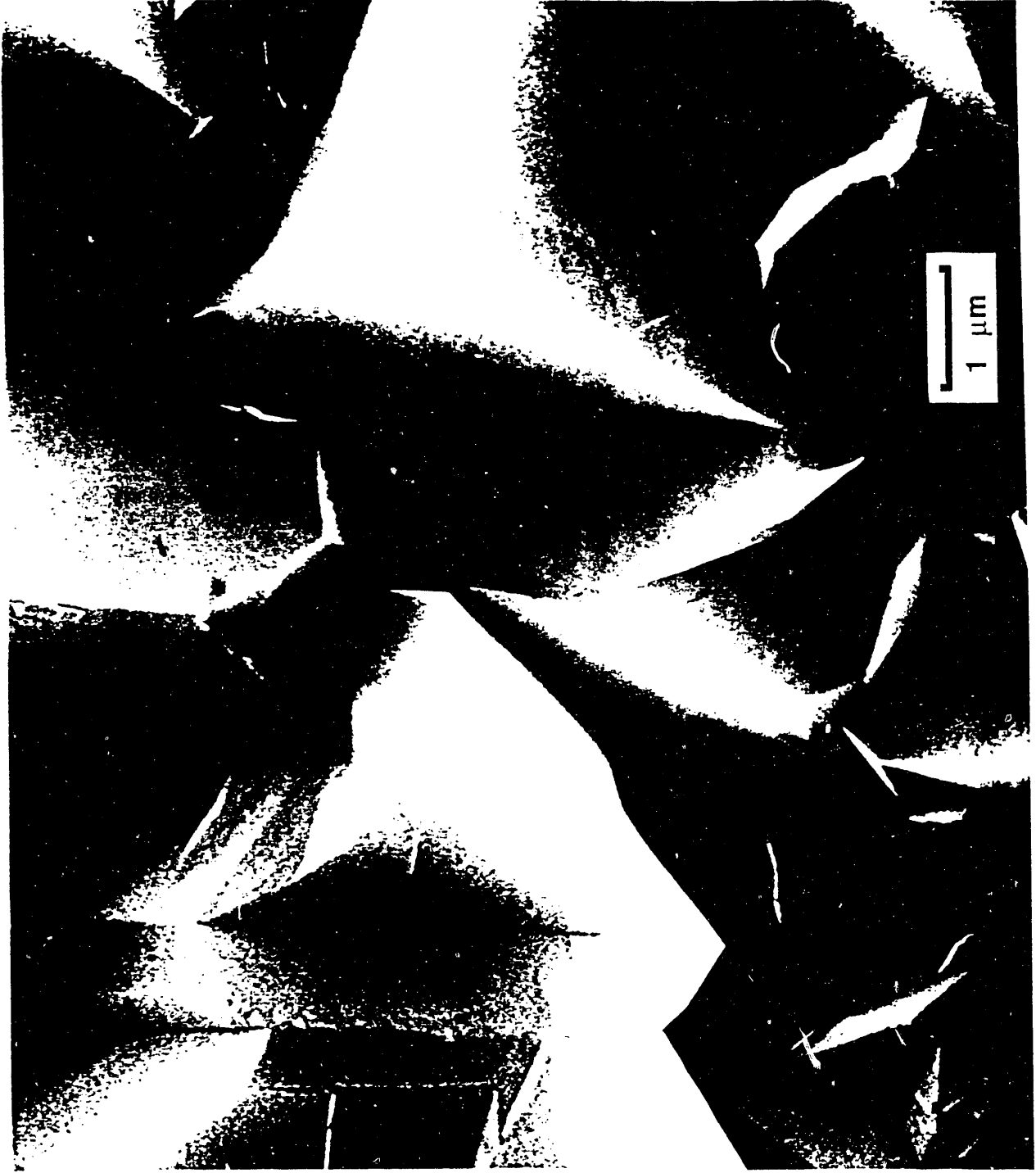


Fig 7

END

**DATE
FILMED**

12102191

